Lithos 118 (2010) 82–94

Contents lists available at ScienceDirect

Lithos

journal homepage: www.elsevier.com/locate/lithos

Trace element partitioning between high-An plagioclase and basaltic to basaltic andesite melt at 1 atmosphere pressure

Frank J. Tepley III [a,*], Craig C. Lundstrom [b], William F. McDonough [c], Amy Thompson [b]

[a] Oregon State University, College of Oceanic and Atmospheric Sciences, 104 COAS Administration Building, Corvallis, OR 97331-5503, United States
[b] University of Illinois, Urbana-Champaign, Department of Geology, 245 Natural History Building, 1301 W. Green Street, Urbana, IL 61801, United States
[c] University of Maryland, Department of Geology, College Park, MD 20742, United States

ARTICLE INFO

Article history:
Received 24 July 2009
Accepted 1 April 2010
Available online 14 April 2010

Keywords:
Partitioning
Plagioclase
Basaltic melt
Trace elements
Differentiation processes

ABSTRACT

We determined plagioclase-melt partition coefficients for 18 elements by performing controlled cooling rate, 1-atmosphere experiments using both natural and synthetic basaltic (51 wt.% SiO_2) and basaltic andesite (56 wt.% SiO_2) powders in a vertical quench furnace. The experiments produced An_{69} to An_{87} composition plagioclase. Three starting powders were Gorda Ridge basalt, synthetic diopside (40%)–albite (28%)–anorthite (32%) mixture, and Arenal volcano (Costa Rica) basaltic andesite. The Gorda and synthetic powders were doped at both low concentrations (20–200 ppm) and high concentration (200–5000 ppm), whereas the Arenal powder was doped only at high concentrations resulting in two doped Gorda powders (low: NP, and high: SDP), two doped diopside/albite/anorthite powders (low: DAD, high: SDD) and one doped Arenal powder (high: AR99-2). Trace elements concentrations in both glass and plagioclase were measured by secondary ion mass spectrometry (SIMS) and/or by laser ablation inductively coupled plasma mass spectrometry (LA-ICP-MS). Results for the partitioning of trace elements between plagioclase and melt at different doping levels demonstrate both adherence to Henry's Law and good agreement between the different analytical techniques. In general, plagioclase-melt partition coefficients determined in the An_{69-73} range are similar to other published values, however, some of those occurring for plagioclase compositions $>An_{75}$ are distinctly lower than those predicted by current regression formulations. We applied a two-lattice melt model to these data to account for differences in melt composition and temperature and found that there were no aberrations associated with partition coefficients. A new set of regression formulations is determined involving the newly determined dataset for plagioclase with An contents between 75 and 87.

1. Introduction

Geochemical modeling of Earth's magmatic processes requires accurate knowledge of trace element partitioning between minerals and co-existing melts. Choosing appropriate partition coefficients for a particular problem is challenging, given that magmatic processes occur over a range of temperatures, pressures, fugacities and melt compositions. Thus, there remains a need for experimental measurements of trace element partitioning at well-documented intensive variables, both to provide absolute values but also to better constrain predictive models of mineral-melt partitioning (e.g. Blundy and Wood, 1994, 2003; van Westrenen and Draper, 2007).

Plagioclase feldspar is a particularly important phase for understanding many magmatic processes. At crustal levels, it is often one of the first phases to crystallize from basaltic magmas, and it strongly influences trace element behavior in crustal-level partial melting processes. Because of these features, plagioclase plays an important role in the development and evolution of oceanic and continental crusts (Kimata et al., 1995; Hansen and Gronvold, 2000; Hellevang and Pedersen, 2008). Most of the recently published plagioclase-melt partition coefficient studies, determined using accurate analytical methods (e.g., secondary ion mass spectrometery (SIMS) or laser ablation inductively coupled plasma mass spectrometry (LA-ICP-MS)), present results for plagioclase compositions in the An_{40} to An_{75} range (e.g., Bindeman et al., 1998). However, mid ocean ridge basalts and oceanic and continental arc rocks often contain plagioclase with An contents >75. Therefore, given the frequent occurrence of $>An_{75}$ plagioclase in natural systems (e.g., Kimata et al., 1995; Lundstrom and Tepley, 2006; Hellevang and Pedersen, 2008), and the complexity of plagioclase-basaltic melt partitioning as a function of both An content and, more notably, the concentration of trace elements in the melt (Bindeman et al., 1998; Bindeman and Davis, 2000; Aigner-Torres et al., 2007), we have undertaken plagioclase-melt partitioning experiments to extend the current range to higher An contents.

This work, therefore, seeks to provide constraints on plagioclase/melt trace element partitioning for natural and synthetic dry basaltic

* Corresponding author. Tel.: +1 541 737 8199; fax: +1 541 737 2064.
E-mail address: ftepley@coas.oregonstate.edu (F.J. Tepley).

0024-4937/$ – see front matter © 2010 Elsevier B.V. All rights reserved.
doi:10.1016/j.lithos.2010.04.001

and basaltic andesite melt compositions at low pressure. Plagioclase compositions range from An_{69} to An_{87} while melts range from 52 to 56 wt.% SiO_2 with data provided for a large suite of trace elements (REE, HFSE, LILE and light elements) doped at ppm levels. This work demonstrates that plagioclase-melt partition coefficients in the $>An_{75}$ range cannot be accurately calculated with published regression lines. Based on this change in partitioning behavior, we calculate new regression line formulations for calculating plagioclase-melt partition coefficients for plagioclase compositions between An_{75} and An_{87}.

2. Experimental and analytical techniques

2.1. Starting materials

Three starting materials were used to investigate trace element partitioning between plagioclase of various An content and melts of differing compositions (Table 1). One set of experiments investigated the trace element partitioning between plagioclase and a mid ocean ridge basalt (~51% SiO_2) from a recent eruption on the Gorda Ridge (Goldstein et al., 1999; Cooper et al., 2003). The starting material for these experiments was a whole rock basalt powder (grain size <40 μm) of the sample analyzed in Cooper et al. (2003). A second set of experiments investigated the plagioclase-melt (~52% SiO_2) partitioning in a basalt analog system (synthetic glass powder of diopside (40%)–albite (28%)–anorthite (32%)) This starting material resulted from grinding of high purity oxides and carbonates followed by de-carbonation, then fusion at 1400 °C for 5 h. An additional experiment resulted from making a 50:50 (by weight) mixture of this synthetic composition and fine-grained albite powder. The last set of experiments determined the partitioning between a more intermediate composition plagioclase and a basaltic andesite derived from Arenal volcano in Costa Rica (AR99-2; Ryder et al., 2006). This whole rock powder was ground by hand under ethanol resulting in a powder with grain size <40 μm. These three compositions were selected with the goal of generating a range of mineral and melt compositions that would, together with existing experimental data, allow us to extend the literature range of partition coefficient data to higher An contents. We doped the starting materials with some trace elements in order to make measurements of elements with low partition coefficients easier and to allow evaluation of Henry's Law behavior.

Many of the elements of interest in this study are incompatible (D_i<0.1) or highly incompatible (D_i<0.01). As a result, experiments on natural concentrations of these elements in mafic melts would likely result in concentrations in plagioclase at or below detection limits for currently available tools. To enable more precise analysis, each of the starting material powders was doped with trace element solutions enriching the material in light elements (Li and B), LILE (Cs, Rb, Ba), REE (La, Nd, Sm, Eu, Er, Yb), HFSE (Zr, Nb, Hf, Ta), and Pb, Th and U. In addition to trace elements doped into the experiments, Sr, and Zr concentrations were high enough to be measured in both plagioclase and glass in all experiments. We doped the Gorda and DAD powders using nitrate solutions to attain two levels of trace element abundances: a low concentration level (20–200 ppm) and a high concentration level (200–1000 ppm). The AR99-2 powder was only doped at the higher trace element level. These steps resulted in two doped Gorda powders (low NP; high: SDP), two doped diopside/albite/anorthite powders (low: DAD; high: SDD), and one doped Arenal powder (high: AR 99-2).

Nitrates were subsequently decomposed by heating at 500 °C for 3 h. This step was critical for the natural starting materials because residual nitrate would react with the Mo foil capsule and compromise the experimental container. However, because this heating step also oxidizes the Fe in the powder, the nitrate solutions were added to only a small aliquot of rock powder that was then heated to decompose the nitrates. This doped powder was then mixed with un-doped powder (in a 5%–95% mixture) by grinding under ethanol until thoroughly mixed and dried resulting in the reported trace element concentrations.

Table 1
Major element composition (wt. %) of starting materials.

	*Di*54-An32-Ab13 + An80 plagioclase	Gorda basalt	Arenal basaltic andesite
	DAD, SDD	NP, SDP	AR99-2
SiO_2	51.95	50.96	55.62
Al_2O_3	22.40	15.67	19.04
Na_2O	1.19	2.69	3.10
MgO	5.69	8.26	4.76
P_2O_5	0.01	0.124	0.18
K_2O	0.20	0.11	0.69
CaO	19.83	11.83	8.80
TiO_2	0.00	1.23	0.62
FeO	0.08	8.20	7.04
MnO	0.00	0.14	0.15
Total	101.06	99.25	99.88

2.2. Experimental and analytical techniques

The experiments were run in the hotspot of a Deltech vertical quench furnace positioned adjacent to a Pt/Pt10%Rh thermocouple calibrated against the melting temperature of Au. The Fe-free synthetic composition samples were run in sealed Pt capsules resulting in uncontrolled but likely highly oxidizing oxygen fugacity. The natural composition experiments, wrapped in Mo foil and sealed inside evacuated silica tubes, experienced an oxygen fugacity buffered between Mo and MoO_2, close to that of iron–wüstite (IW) and thus reducing.

The pertinent phase relationships were first determined for each starting material. For the subsequent partitioning experiments, samples were held above the liquidus for 48–72 h and ramped at a rate of 2°/h to the pre-determined crystallization temperature (generally a few degrees below the liquidus). Table 2 gives the temperature–time paths of individual experiments. Once this temperature was reached, samples were held for 24–72 h to provide ample time for plagioclase crystallization, which is known to be kinetically sluggish (Grove et al. 1984), particularly in dry systems. Samples were then quenched in water, mounted in epoxy, polished and inspected for crystals and glass.

Both wavelength dispersive spectroscopy (WDS) electron microprobe analysis and energy dispersive spectroscopy (EDS) scanning electron microscope analysis were used to determine major element phase compositions. The WDS analyses were performed on a Cameca SX-50 electron microprobe at the University of Chicago using a 15 kV accelerating voltage and 10 nA probe current with calibration based on well-characterized mineral and oxides standards. Step sizes during traverses range from 5 to 20 μm for a duration of 10 s/analysis (e.g., Steele et al., 1997). The EDS analyses were performed on a JEOL 840A SEM using standards based analysis on a 4Pi digital processing system at the University of Illinois, Urbana-Champaign (UIUC). Analysis of Lake County plagioclase and VG-2 basaltic glass indicate the accuracy of the EDS analyses (Table 3).

Trace elements were determined by either of two methods: 1) SIMS or 2) LA-ICP-MS. SIMS analyses were run on a Cameca IMS 5f located in the Department of Energy/University of Illinois, Urbana-Champaign Center for Microanalysis of Materials in the Frederick Seitz Materials Research Laboratory. A 12.5 kV primary beam of oxygen ions (current of 10–20 nA) was directed at the sample and positive secondary ions were accelerated to 4.5 keV with an energy filtering technique applied to minimize molecular interferences (Shimizu et al., 1978; Zinner and Crozaz, 1986;). An offset energy of 75 V with an energy window of ±30 eV was used. Isotopes used for measurement include ^{7}Li, ^{11}B, ^{30}Si, ^{39}K, ^{133}Cs, ^{85}Rb, ^{88}Sr, ^{90}Zr, ^{138}Ba, ^{139}La, ^{142}Nd, ^{152}Sm, ^{153}Eu, ^{166}Er, ^{174}Yb, ^{91}Nb, ^{180}Hf, ^{181}Ta, ^{232}Th and ^{238}U.

Table 2
Summary of experimental conditions.

Experiment	Loading T	Begin ramp	Cooling rate	Quench T	Duration	Modal abundances			Crystal width
	T (°C)	*T* (°C)	(°h^{-1})	T(°C)	(h)	pl	ol	gl	(mm)
NP4	1239	1200	2	1180	58	20	5	75	100–300
NP5	1235	1200	2	1176	95	20	5	75	100–300
SDP	1240	1200	2	1142	45	20	5	75	100–300
DAD1	1394	1300	2	1264	161	5	–	95	50–100
DAD2	1393	1300	2	1263	122	10	–	90	50–100
SDD	1383	1303	2	1265	96	15	–	85	50–100
AR 99-2	1220	1190	2	1127	115	7	–	93	100–200

Counts were ratioed to ^{30}Si. Partition coefficients were calculated by dividing the average ^{30}Si-normalized count rates of each measured isotope in the plagioclase by the corresponding ^{30}Si-normalized count rate in the glass and correcting for the slight difference in SiO_2 contents of the two phases. Partition coefficients are reported in Table 4. Trace element concentrations in the glasses were calculated from the useful yields determined based on the trace element concentration within NIST610 or KLG-2 basaltic glass standard. Accuracy of trace element concentrations is estimated at ±30%.

LA-ICP-MS analyses were run on a Finnigan ELEMENT 2 ICP-MS coupled to either a ArF charged, excimer laser (Compex 110, Lambda Physik) operating at 10 Hz or a 5th harmonic Nd:YAG laser (UP-213, New Wave Research) operating at 10 Hz in the Department of Geology at the University of Maryland (UM). All trace element ion intensities were normalized to ^{43}Ca intensities and converted to concentrations based on the known CaO content of the phase (Table 3). Spot size was generally ~20–30 μm in the glass and as small as 8 μm in crystals. Analyses consisted of ~20 s of background monitoring with the laser off followed by 10–20 s of magnet scans collecting the ablated sample. However, processing of the data resulted in shorter collection intervals as the small crystals were rapidly ablated. Calibration was performed relative to NIST 610 with several BCR-2 analyses per day used to check accuracy. Trace element concentrations measured by SIMS at UIUC and by LA-ICP-MS at UM on common samples were shown to be in excellent agreement by Huang et al. (2006).

3. Results

3.1. Major element composition of phases

We report the results of seven partition coefficient experiments between basaltic to basaltic andesite melt compositions and co-existing plagioclase phenocrysts in dry and low pressure conditions. The experiments are ideal for partition coefficient determination owing to their low degree of total crystallinity and lack of significant crystallization of other phases (Table 2). Plagioclase crystals in the experiments have euhedral forms (Fig. 1), with the DAD charges producing ~5–15% modal plagioclase (An_{87}) as 50–100-μm width crystals co-existing with a haplobasaltic melt at ~1264 °C (DAD and SDD). The Gorda basalt experiments produced ~20% modal $An_{74–76}$ plagioclase of crystal size 100–300 μm and minor (5% modal) olivine co-existing with basaltic melt at ~1178 °C and ~1142 °C, respectively (NP and SDP). A single experimental run of doped AR99-2 produced ~5–10% modal plagioclase (An_{69}) co-existing with basaltic andesite melt at ~1127 °C (AR99-2).

Table 3
Comparison of major element analyses of plagioclase and co-existing glass determined through EDS and WDS analyses.

Method PLAGIOCLASE	EDS Lake County plagioclase		EDS accepted value	EDS DAD-1		EDS DAD-2		EDS SDD-1		EDS NP-4		EDS NP-5		WDS SDP-9		EDS AR99-2	
SiO_2	51.47	0.13	51.25	46.25	0.52	46.14	0.08	46.45	0.07	49.63	0.01	49.77	0.01	51.99	0.01	53.24	0.03
Al_2O_3	30.98	0.08	30.91	33.62	0.32	33.83	0.06	33.87	0.11	31.84	0.02	31.77	0.02	29.97	0.05	29.67	0.05
FeO	0.4	0.07	0.46	0.06	0.05	0.04	0.04	0.03	0.01	0.28	0.04	0.39	0.08	0.28	0.15	0.39	0.16
CaO	13.78	0.04	13.64	18.38	0.43	18.43	0.02	18.15	0.15	15.7	0.02	15.36	0.05	14.69	0.37	13.3	0.47
Na_2O	3.25	0.05	3.45	1.47	0.08	1.43	0.07	1.45	0.06	2.5	0.10	2.64	0.04	3.01	0.31	3.17	0.36
K_2O	0.13	0.02	0.18	0.21	0.05	0.13	0.02	0.05	0.03	0.04	0.08	0.07	0.09	0.05	1.11	0.23	0.63
Si				2.14		2.13		2.14		2.27		2.27		2.37		2.41	
Al				1.83		1.84		1.84		1.72		1.71		1.61		1.58	
Fe^{+2}				0.00		0.00		0.00		0.01		0.02		0.01		0.02	
Ca				0.91		0.91		0.90		0.77		0.75		0.72		0.65	
Na				0.13		0.13		0.13		0.22		0.23		0.27		0.28	
K				0.01		0.01		0.00		0.00		0.00		0.00		0.01	
Total cations				5.02		5.02		5.01		4.99		4.99		4.97		4.94	
An content				86		87		87		77		76		74		69	
Method GLASS	EDS Basaltic glass VG-2		Accepted value	WDS DAD-1		WDS DAD-2		EDS SDD-1		WDS NP-4		WDS NP-5		WDS SDP-9		EDS AR99-2	
SiO_2	50.27	0.03	50.81	54.43	0.42	54.64	0.13	54.42	0.13	51.97	0.37	52.23	0.52	54.63	0.62	56.31	0.28
Al_2O_3	14.50	0.04	14.06	17.07	0.19	16.94	0.10	17.29	0.13	16.61	0.17	16.28	0.11	12.69	0.09	17.45	0.06
FeO	12.07	0.01	11.84	0.06	0.03	0.04	0.03	0.05	0.03	7.59	0.10	7.65	0.14	9.29	0.18	7.51	0.08
MgO	7.54	0.04	6.71	8.42	0.07	8.52	0.05	8.21	0.07	8.43	0.12	8.43	0.08	6.83	0.09	6.73	0.04
CaO	11.21	0.02	11.12	18.50	0.10	18.33	0.10	18.54	0.10	11.91	0.09	11.78	0.07	12.49	0.23	8.11	0.10
Na_2O	2.50	0.08	2.62	1.23	0.04	1.24	0.02	1.24	0.02	2.13	0.03	2.34	0.03	1.97	0.09	2.44	0.01
K_2O	0.16	0.02	0.19	0.27	0.02	0.28	0.03	0.26	0.03	0.19	0.01	0.15	0.01	0.22	0.01	0.73	0.05
TiO_2	1.75	0.03	1.85	0.01	0.01	0.01	0.01	0.00	0.01	1.17	0.03	1.16	0.02	1.89	0.17	0.70	0.04
WDS total:				99.76		98.04				98.63		99.13		98.01			

Table 4
Glass concentrations and $D^{plag/liquid}$ for experimental runs.

Laser ablation ICP-MS

	NP4 Glass (ppm)	$D^{plag/liquid}$	NP5 glass (ppm)	$D^{plag/liquid}$	SDP9 glass (ppm)	$D^{plag/liquid}$	DAD-1 glass (ppm)	$D^{plag/liquid}$	DAD-2 glass (ppm)	$D^{plag/liquid}$	AR99-2 glass (ppm)	$D^{plag/liquid}$
Ti	1.1 (0.027)	0.0454 (0.016)	1.172 (0.120)	0.042 (0.013)	1.6 (0.041)	0.0441 (0.013)					0.7 (0.002)	0.0470 (0.0097)
Rb					467.2 (5.905)	0.0207 (0.014)	246.1 (0.946)	*0.0174*	268 (2.254)	0.021 (0.0150)	444.3 (13.146)	0.0180 (0.0014)
Sr	147.0 (8.255)	1.7863 (0.446)	150 (8.728)	1.863 (0.178)	130.9 (0.568)	2.0796 (0.183)	59.5 (1.860)	1.1904 (0.0565)	60 (1.428)	1.029 (0.1888)	596.8 (10.049)	1.9447 (0.1665)
Zr			71 (10.437)	0.012 (0.006)	110.6 (4.165)	0.0108 (0.010)	23.4 (0.158)	0.0020 (0.0028)	22 (0.871)	*0.010*	44.9 (4.380)	0.0039 (0.0027)
Nb	97.9 (4.172)	0.0054 (0.004)	112 (13.095)	0.002 (0.003)	422.8 (11.307)	*0.0014*	106.9 (0.423)	0.0011 (0.0016)				
Cs			78 (11.594)	0.019 (0.004)	679.0 (13.177)	0.0039 (0.002)					479.2 (39.013)	0.0060 (0.0067)
Ba			38 (10.654)	0.270 (0.207)	420.4 (9.543)	0.2309 (0.037)	33.6 (2.007)	0.1410 (0.0217)	70 (2.002)	0.157 (0.0226)	997.3 (111.810)	0.3204 (0.0434)
La	25.8 (1.897)	*0.0554*	29 (3.422)	0.088 (0.017)	203.3 (2.833)	0.0517 (0.011)	56.3 (0.155)	0.0374 (0.0064)	118 (0.602)	0.032 (0.0051)	59.7 (1.951)	0.1096 (0.0427)
Ce			9 (1.338)	0.056 (0.032)	11.9 (0.048)	0.0400 (0.008)					16.4 (0.573)	0.0367 (0.0289)
Nd			6 (3.187)	0.045	497.2 (5.573)	0.0369 (0.021)	52.6 (0.601)	*0.0247*	108 (1.997)	0.021 (0.0162)	254.1 (0.174)	0.0506 (0.0037)
Sm					584.2 (9.181)	0.0176 (0.011)	53.3 (0.273)	*0.0100*	107 (1.005)	*0.008*	256.9 (10.956)	0.0413 (0.0031)
Eu	25.3 (1.359)	1.0250 (0.093)	27 (1.712)	0.942 (0.135)	149.0 (1.910)	0.9606 (0.160)	56.9 (0.250)	0.0149 (0.0052)	114 (1.623)	0.015 (0.0062)	95.0 (0.862)	1.4160 (0.0346)
Tb					1.0 (0.111)							
Er	22.9 (6.692)	*0.0362*	24 (6.722)	0.012 (0.004)	510.8 (15.999)	0.0050 (0.005)	55.3 (0.138)	*0.0024*	103 (4.914)	0.004 (0.0046)	183.1 (39.138)	0.0053 (0.0075)
Yb			32 (6.051)	0.008 (0.010)								
Hf					174.5 (3.828)	0.0009 (0.002)					54.1 (11.994)	*0.0015*
Ta	79.5 (9.796)	*0.0020*	89 (4.808)	0.001	381.9 (6.015)	0.0008 (0.001)			123 (2.180)	0.001 (0.0005)	208.4 (1.655)	0.0003 (0.0005)
Pb	43.4 (4.699)	0.1621 (0.043)	54 (4.881)	0.112 (0.021)	647.5 (17.392)	0.0944 (0.011)	*69.6 (1.888)*	*0.0726 (0.0028)*	61(3.625)	*0.181 (0.0669)*	338.1 (2.327)	*0.1085*
Th	124.2 (22.102)	0.0003 (0.001)			388.4 (7.740)	0.0002 (0.0003)	308.4 (3.240)	0.0002 (0.0002)	396 (22)	0.0001 (0.0001)	175.9 (10.300)	0.0001 (0.0001)
U	36.6 (1.915)	0.0013 (0.002)			1006.5 (20.517)	<0.0001					564.1 (20.345)	0.0002 (0.0002)

SIMS

	SDD (a) glass (ppm)	$D^{plag/liquid}$ (a)	SDD (b) glass (ppm)	$D^{plag/liquid}$ (b)	DAD-1 glass (ppm)	$D^{plag/liquid}$
Li		0.1812 (0.008)		0.1999 (0.011)		0.2970 (0.053)
B		0.0474 (0.063		0.0298 (0.046		0.0135 (0.0048)
P				0.3643 (0.115)		
K				0.0870 (0.019)		0.1615 (0.0116)
Ti		0.7638 (0.112)				
Rb	2564 (200.533)	0.0131 (0.002)			403 (28.998)	0.0185 (0.002)
Sr	157 (4.936)	0.9938 (0.039)			149 (1.351)	1.0490 (0.083)
Zr		0.0034 (0.0029)				
Nb			3223 (55.456)	0.0007 (0.0002)		
Cs				0.0045 (0.0046)		
Ba	1742 (84.199)	0.1262 (0.013)	1741 (20.312)	0.1242 (0.023)	102 (8.909)	0.0873 (0.0078)
La	1824 (50.793)	0.0330 (0.004)	1795 (104.922)	0.0311 (0.004)	169 (2.944)	0.0348 (0.0036)
Nd	3434 (206.367)	0.0190 (0.0013)			112 (12.725)	0.0243 (0.003)
Eu				0.0136 (0.001)	49 (1.411)	0.0145 (0.0023)
Eu	580 (2.959)	0.0153 (0.0012)	577 (15.952)	0.0154 (0.002)		
Sm	4939 (141.913)	0.0123 (0013)	4784 (294.588)	0.0137 (0.002)	174 (1.341)	0.0140 (0.0003)
Er		0.0046 (0.0007)				0.0057 (0.0015)
Yb	7 (0.233)	0.0030 (0.0004)			0.27 (0.008)	0.0027 (0.0004)
Hf	2204 (115.947)	0.0010 (0.0003)				
Ta			2883 (64.151)	0.0009 (0.0004)		
Th			6391 (216.259)	0.0004 (0.0003)	1003 (28.392)	0.0002 (0.00002)
U			6215 (165.450)	0.0003 (0.0002)	224 (4.618)	0.00004 (0.00001)

Numbers in parentheses are 1-sigma errors. Italicized numbers represent questionable data.

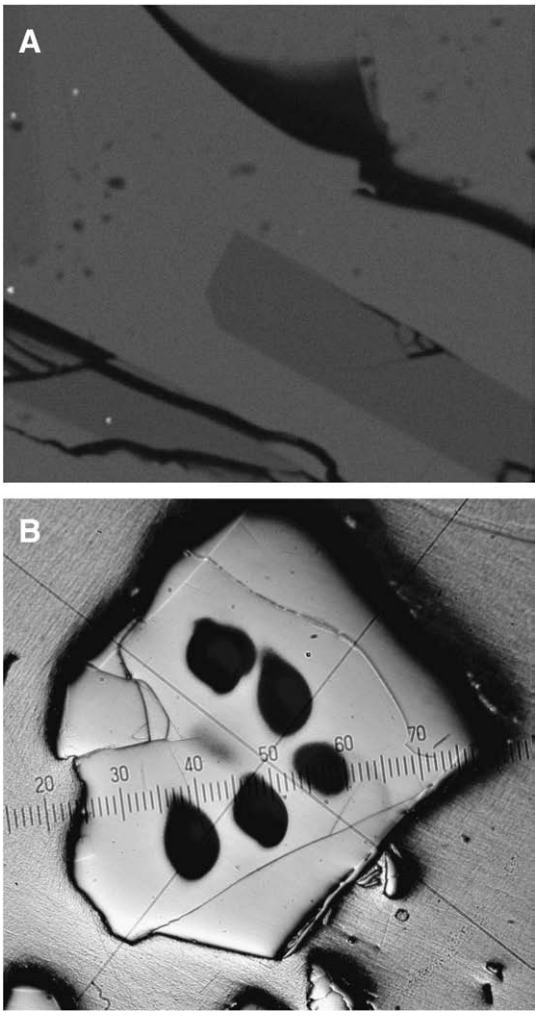

Fig. 1. (A) Back scatter electron image (BSE) of plagioclase and glass from experiment SDP 9. Note euhedral crystal morphology and absence of trapped melt within the crystal. Field of view is 60 mm. (B) Reflected light image of quenched glass with SIMS craters. Field of view is 1 mm.

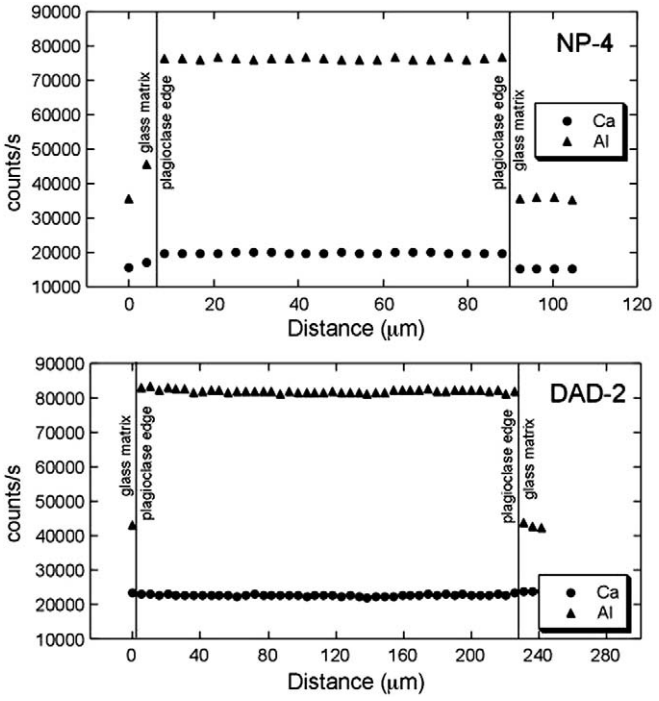

Fig. 2. Electron microprobe transects across plagioclase crystals for experiments NP-4 and DAD-2. Shown is representative Ca and Al counts per second transects across plagioclase crystals illustrating the lack of compositional zoning. Each spot represents one "analysis" with 10-s counting times. Based on methodology of Steele et al. (1997).

Melt compositions vary over a fairly narrow range in SiO_2 content, from ~51 wt.% in the Gorda ridge basalt up to ~56% in the Arenal basaltic andesite. The major difference between melt compositions reflects the CaO contents which are at natural magma levels of 12 to 12.5 wt.% in the Gorda and Arenal starting materials to a strongly elevated ~18.5 wt.% in the synthetic diopside–albite–anorthite starting material.

Both glass and plagioclase compositions are invariant within standard deviations within a single experiment. Several analytical traverses across plagioclase crystals indicate no major element zoning (Fig. 2). The standard deviation of SIMS analyses of the glass also indicates trace element homogeneity of the melts. Finally, the plagioclase/melt Na–Ca exchange coefficient ($^{Ca-Na}K_D = [^{xtal}X_{Ca}][^{melt}X_{Na}]/[^{xtal}X_{Na}][^{melt}X_{Ca}]$) is in good agreement with previous studies; for the two natural starting compositions, the value ranges between 1.12 and 1.26, consistent with values observed in previous natural composition "dry" experiments on basalt to andesite compositions (Tormey et al., 1987; Bartels et al., 1991). In contrast, a systematic offset in the $^{Ca-Na}K_D$ of the synthetic system to lower values for the exchange coefficient is apparent.

3.2. Trace element partitioning

Trace element concentrations in run products and calculated partition coefficients for plagioclase/glass pairs are listed in Table 4. Partition coefficients for REE increase from HREE (0.008 to 0.003) to LREE (0.055 to 0.032). LILE partition coefficients range from ~2 for Sr to lower values for Cs, Rb, K and Ba (0.18 to 0.005). Finally, partition coefficients for the light elements range from $D_{Li} = 0.4$ to $D_B = 0.02$. D_U and D_{Th} vary between 0.0002 and 0.0005.

In this study, we have employed two different analytical techniques (SIMS and LA-ICP-MS), allowing us to compare the different techniques. Results for DAD-1, a sample in which both techniques were used to measure trace element concentrations, indicate good agreement between the two techniques for a variety of elements (Table 5).

Separate experiments using the same starting material at the same temperatures (e.g., DAD-1 and DAD-2 or NP-4 and NP-5) show good agreement for all partition coefficients. For example, partition coefficients for Sr, Ba, La and Eu in DAD-1 and DAD-2, differ by between 11 and 16% relative, well within the analytical uncertainty (±30%). Similarly, the partition coefficients for Ti, Sr and Eu in NP-4 and NP-5, vary between 6 and 9%, well within analytical uncertainty, although the larger uncertainties on other elements (e.g., La, Pb and Er) limits this comparison.

Table 5
Comparison of $D^{plag/liquid}$ of various elements from the same experiment (DAD-1) with different measurement methods.

Element	LA-ICP-MS	SIMS
Rb	0.0174	0.0185
Sr	1.1904	1.0490
Ba	0.1410	0.0873
La	0.0374	0.0348
Nd	0.0247	0.0243
Sm	0.0100	0.0140
Eu	0.0149	0.0145
Er	0.0024	0.0057
Th	0.0002	0.0002

3.3. Variations in Ds with doping level

There have been several recent papers discussing the role of doping level in determining plagioclase-melt partition coefficients (Bindeman et al., 1998; Bindeman and Davis, 2000). These follow up on studies which established that Henry's Law behavior in general is followed in experiment with up to single wt.% levels of doping (Watson, 1985; McKay, 1986; Beattie, 1994). However, Bindeman et al. (1998) and Bindeman and Davis (2000) observed non-Henry's Law behavior associated with high levels of doping for the determination of D_{REE}. They argue that this reflects the crystal chemical control of substituting trace cations largely competing for sites of substitution with the mineral-forming cations Na and Ca.

In the interest of exploring this further, we used starting materials with a range in trace element concentration similar to that in Bindeman et al. (1998) and Bindeman and Davis (2000). This included two doping levels each of the natural Gorda basalt sample (NP and SDP) and the synthetic mix sample (DAD and SDD). Fig. 3 shows the partition coefficients for selected alkaline earth elements and rare earth elements from the synthetic mix samples as a function of trace element concentration. In the synthetic starting material, trace element concentrations in the melt varied between <100 ppm and ~5000 ppm, close to that in many previous studies (e.g., Lundstrom et al., 1994; Bindeman et al., 1998; Barth et al., 2002), and well below threshold levels for Henry's Law behavior in the studies of Watson (1985), McKay (1986) and Beattie (1994). As the figure illustrates, the partition coefficients are constant over the range in doping level with excellent analytical precisions under low and medium doping concentrations. These observations suggest that deviation from Henry's Law did not occur in these samples and experiments.

3.4. Regressions of $RT\ln D_i$ versus An content

Trace element partition coefficients are integral factors in modeling magmatic processes such as fractional crystallization and partial melting. However, magmatic differentiation processes are complex and in many cases involve unknown intensive and extensive variables. Because partition coefficients cannot be determined for every condition, much effort has been directed toward predicting partitioning behavior using both thermodynamic and empirical formulations. In the case of trace element partitioning between plagioclase and dry melt, there are little data to constrain partitioning behavior at $>An_{80}$ plagioclase composition, despite abundant observation of such plagioclase compositions in Earth's magmas. One way to constrain the relevant D's for high-An plagioclase is to use the linear relationship between An content in plagioclase and $RT\ln D_i$ to predict

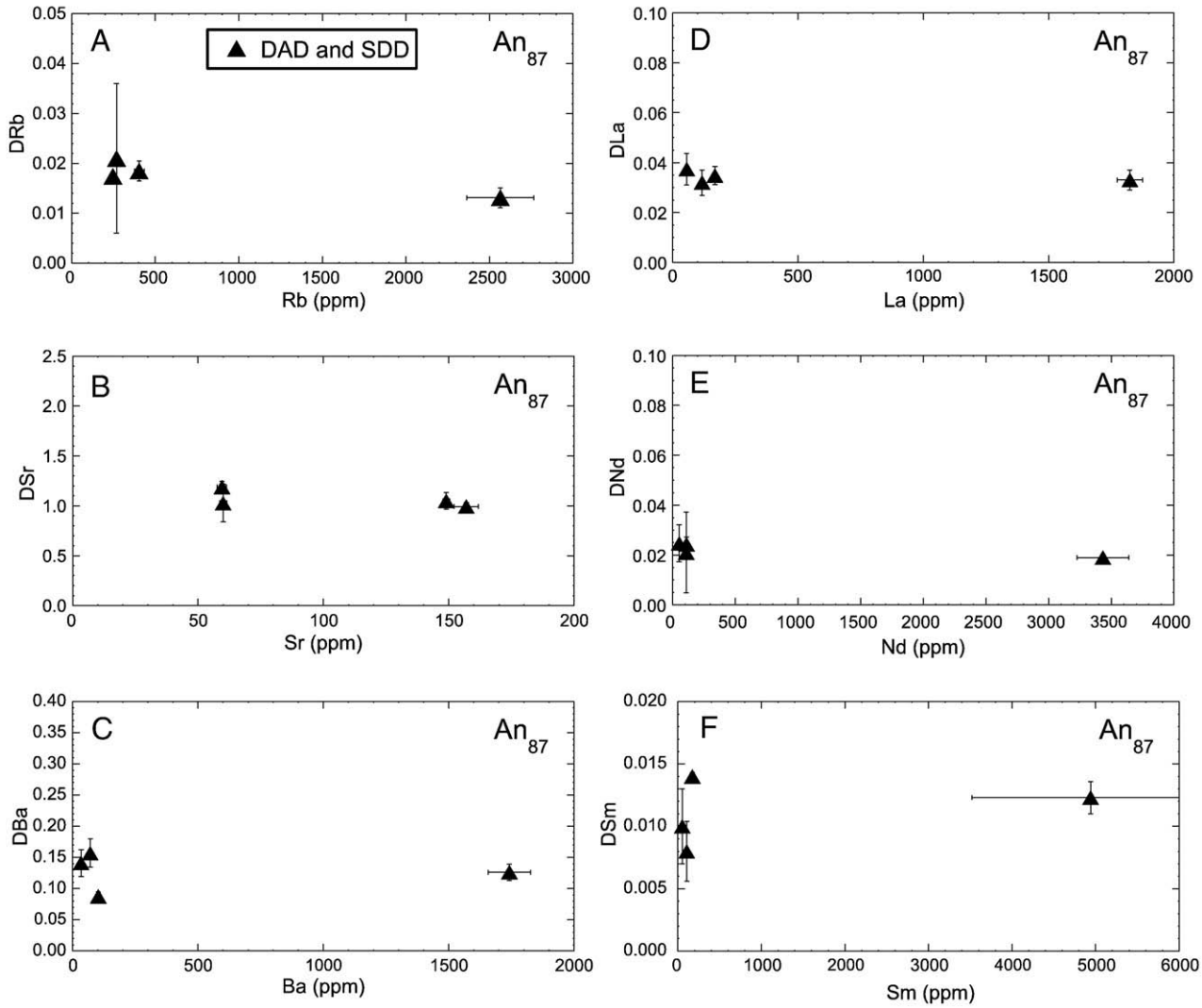

Fig. 3. Plagioclase-melt partition coefficients for selected trace elements in DAD and SDD synthetic experiments between melt and An_{87} composition plagioclase as a function of trace element concentration. As can be seen, partition coefficients are within error of each other for various trace elements at low and high trace element doping levels indicating adherence to Henry's Law.

partition coefficients above An_{80}. However, the fact that most of the data describing the linear relationship come from < An_{80} plagioclase and that much of the data show considerable scatter makes these conclusions problematic. Our experiments provide direct constraints on partitioning involving high-An plagioclase.

Blundy and Wood (1991) developed a general equation for the partitioning of Sr and Ba into plagioclase, showing that $RT\ln D_i$ was linearly dependent on An content:

$$RT \ln D_i = Y - X * X_{An} \quad (1)$$

where R is the gas constant, X_{An} is the anorthite mole fraction in plagioclase, T is temperature in K, X is the slope and Y is the intercept in a regression plot of $RT\ln D_i$ versus X_{An}. With more recent data, Bindeman et al. (1998), Bindeman and Davis (2000), Bédard (2006) and Bindeman (2007) continue to find this linear dependency on An content. As all of these authors point out, there is a small temperature effect on plagioclase-melt partition coefficients, therefore $RT\ln D_i$ is plotted to minimize this effect (Blundy and Wood, 1991). We also adopt this convention, and use it to compare our results with these previous studies. However we limit the comparison to data measured with either SIMS or LA-ICP-MS techniques in dry natural or synthetic systems with An content ranging from An_{50} to An_{100}. Based on these criteria, we use the datasets of Bindeman et al. (1998), Bindeman and Davis (2000), and Aigner-Torres et al. (2007), and compare the regression equations from Blundy and Wood (1991), Bindeman et al. (1998), Bédard (2006) and Bindeman et al. (2007). The dataset of Miller at al. (2006) is used to illustrate the effect of melt chemistry on Sr and Ba mineral-melt partition coefficients but is not used in determining new regression equations. Furthermore, we do not use the dataset produced from lunar samples (e.g., Weill and McKay, 1975; McKay and Weill, 1977; Ringwood, 1970) as we are focusing on terrestrial magmatic processes. We produce linear regressions for two data sets: 1) "all data" is a combined data set inclusive of data from the references above and from this study; 2) a data set exclusively determined from this study. Table 6 lists the regression equations for each element determined from partition coefficients determined in this study with slope (X) and its error (x) and the intercept (Y) and its error (y) based on least squares methodology (LINEST function in Excel™).

Table 6
Regression results for plagioclase-melt partition coefficients.

Element	Y intercept	$\pm Y$	R^2	Slope (X)	$\pm X$	Eq.#
*RT*ln*DSr*	44,453	1303	0.90	−501.8	68.8	2
RTlnDRb	−20,871	2437	0.63	−357	138	3
RTlnDBa	41,618	2964	0.83	−786	161	4
*RT*ln*DPb*	−15,761	5484	0.03	−132	444	5
*RT*ln*DLa*	37,900	2319	0.91	−937	122	6
*RT*ln*DNd*	24,365	1492	0.96	−843	81	7
*RT*ln*DSm*	35,372	3106	0.90	−1080	175.4	8
*RT*ln*DZr*	−7042	10,188	0.27	−709	582	9
*RT*ln*DTh*	−60,465	6073	0.40	−581	355	10
*RT*ln*DTi*	−14,204	493	0.87	−309	86	11

3.4.1. LILE and alkaline earth elements (Sr, Rb, Ba, Pb)

The behavior of Sr is most consistent with control by plagioclase An content while other LILE indicate more poor correlations. For Sr, a linear regression of *RT*ln*DSr* versus An content (Fig. 4A) for all data has an R^2 of 0.84 with the slope and intercept similar to that Bindeman et al. (1998). However, the slope of the regression line for data from this study is considerably steeper with a high degree of correlation ($R^2 = 0.90$). The steeper slope mostly reflects the low partition coefficients for Sr in the synthetic diopside–albite–anorthite starting material with DSr for plagioclase of similar An content to Bindeman et al. (1998), Bindeman and Davis (2000) and Aigner-Torres et al. (2007) producing similar partition coefficients. Also plotted on this diagram are the partition coefficients for An_{100} plagioclase from Miller et al. (2006) to illustrate the effect of melt composition on partitioning. Rb shows less systematic behavior with *RT*ln*DRb* versus An content (Fig. 4B) producing a poor correlation ($R^2 = 0.25$). The regression for data from this study produces a similar slope to previous regressions (Bindeman et al. (1998); Bédard (2006) but with better correlation ($R^2 = 0.63$). Similarly, *RT*ln*DBa* for data from all studies (Fig. 4C) shows poor correlation ($R^2 = 0.56$). Again, data from this study at higher An content plot below the regression line through all the data, whereas those with intermediate An content are similar to the data from other studies. Regression lines from Bédard (2006), Blundy and Wood (1991) and Bindeman et al (1998) have similar slopes that converge near An_{50}. Data from higher An content of this study lie along the Bindeman et al. (1998) regression line. A regression line plotted through the data from this study alone has a steeper slope and has a good correlation ($R^2 = 0.83$). For Pb, regression lines produced from the data of Bindeman et al (1998) and Bindeman and Davis (2000) are nearly coincident with the regression line of Bédard (2006) (Fig. 4D), although the data show large variability. Data from this study plot below these regression lines and have a poor correlation ($R^2 = 0.03$), however, when combined with all the data, they have a correlation that is acceptable ($R^2 = 0.41$).

3.4.2. REE (La, Nd, Sm)

In comparison to the partition coefficients from the other studies, the D_{REE} from this study consistently are lower for plagioclase in the An_{69} to An_{80} range. Furthermore the D_{REE} from An_{87} are well below regression lines of Bindeman et al (1998) and Bédard (2006) (Fig. 4E–G). This follows a similar trend of lower Ds for higher An contents that is shown by the LILE and alkaline earth elements. When all the data are binned together, regressions lines have poor to average correlations ($R^2 = 0.38$ to 0.66). When data from this study are considered independently, the regression lines exhibit very good to excellent correlations ($R^2 = 0.90$ to 0.96).

3.4.3. HFSE (Zr, Th, Ti)

In the case of *RT*ln*DZr*, the data from this study tend to plot above other comparable data and above regression lines from similar studies (Fig. 4 H). A regression line fit through all data shows no correlation ($R^2 = 0.03$). However, a regression line fit through our data exclusively produces a poor correlation ($R^2 = 0.27$). This regression line is also similar to the regression lines of Bindeman et al. (1998) and Bédard (2006). There are no data from Bindeman et al. (1998) that can be used for comparison to our data for *RT*ln*DTh*, however a regression line through our data, with poor correlation ($R^2 = 0.40$), parallels a regression line from Bédard (2006) with lower intercept values (Fig. 4I). Lastly, data for D_{Ti} from this study are limited to plagioclase compositions between An_{69} and An_{76}. On a *RT*ln*DTi* versus An content plot, these data are coincident with data from other studies (Fig. 4J). Regression lines through the total dataset produce an average correlation ($R^2 = 0.76$), whereas the correlation for a line through

Fig. 4. (A) RTlnDSr, (B) RTlnDRb, (C) RTlnDBa, (D) RTlnDPb, (E) RTlnDLa, (F) RTlnDNd, (G) RTlnDSm, (H) RTlnDZr, (I) RTlnDTh and (J) RTlnDTi versus An content. Each diagram illustrates (1) a regression formulation based a combined dataset "all data" of partition coefficient determined from this study and published partition coefficients that qualify within our criteria (BDD98: Bindeman et al., 1998; BD00: Bindeman and Davis, 2000; AT07: Aigner-Torres et al., 2007), and (2) multiple regression formulations based on separation of these data. In the separated data regressions, regression formulations for this study are designated with a black dashed line whereas those of other studies are designated with thin solid lines (Bed06: Bédard, 2006; BDD98: Bindeman et al., 1998; BD00: Bindeman and Davis, 2000; BW91: Blundy and Wood, 1991). Included in the RTlnDSr plot are data from Miller et al. (2006) (M06).

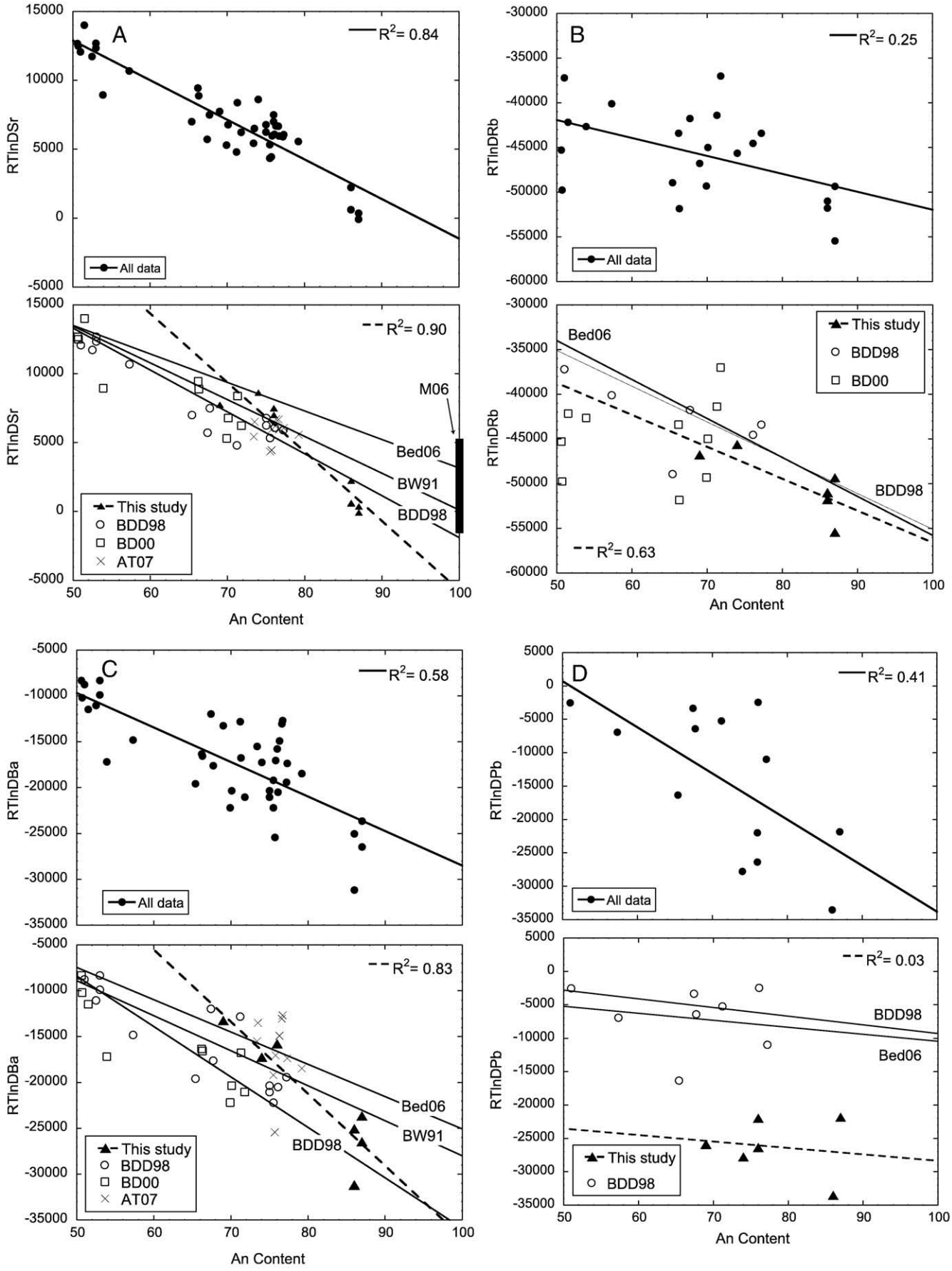
A
R²= 0.84
All data
RTInDSr
B
R²= 0.25
All data
RTInDRb
R²= 0.90
M06
Bed06
BW91
BDD98
This study
BDD98
BD00
AT07
RTInDSr
Bed06
BDD98
This study
BDD98
BD00
R²= 0.63
RTInDRb
An Content
An Content
C
R²= 0.58
All data
RTInDBa
D
R²= 0.41
All data
RTInDPb
R²= 0.83
Bed06
BW91
BDD98
This study
BDD98
BD00
AT07
RTInDBa
R²= 0.03
BDD98
Bed06
This study
BDD98
RTInDPb
An Content
An Content

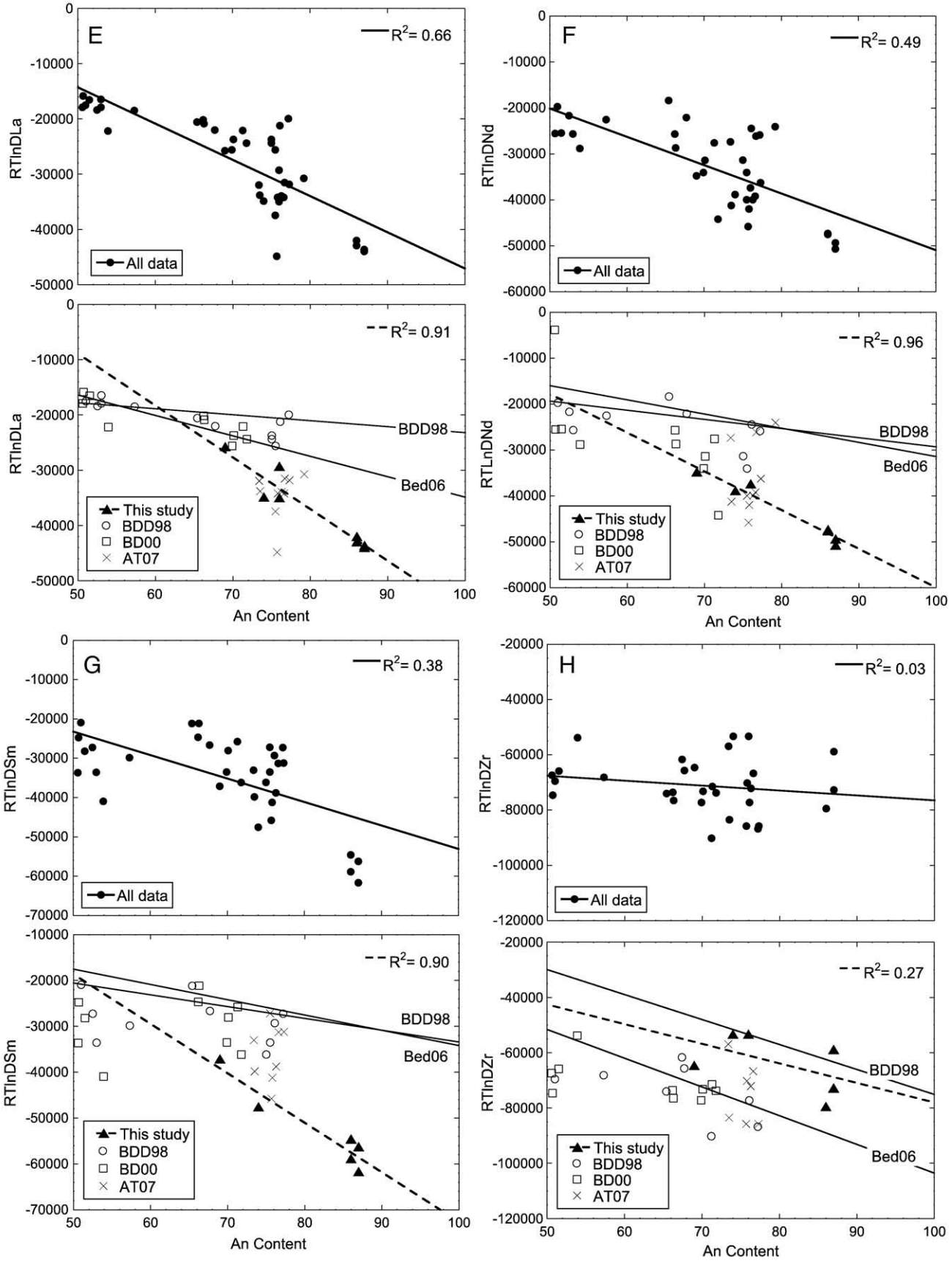

Fig. 4 (*continued*).

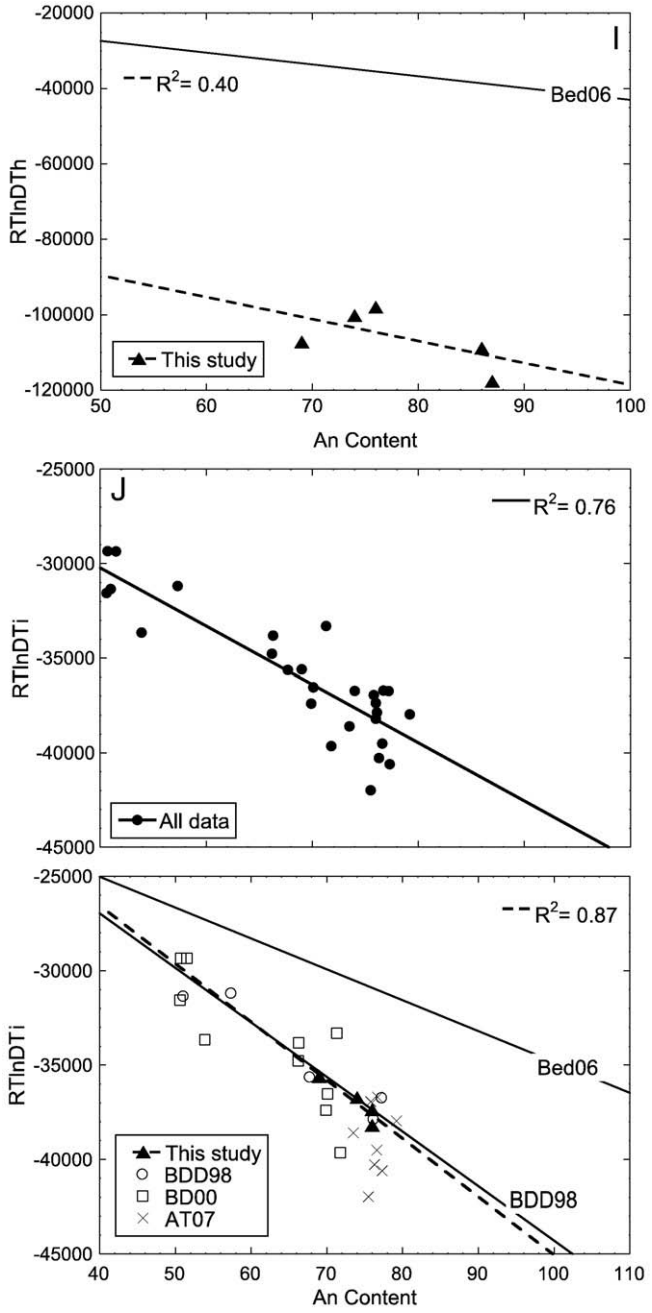

Fig. 4 (*continued*).

our data is good ($R^2 = 0.87$), and the line is nearly coincident with the line of Bindeman et al. (1998).

4. Discussion

4.1. Assessment of equilibrium

Although we have not attempted reversal experiments in this study, several lines of evidence point to our measured partition coefficients representing equilibrium values. First, there is no discernible major element zoning within either the melt or crystal phases of these experiments Fig. 2). This is observed in a lack of major element variations across the crystals and in the low standard deviations in glass analyses via SIMS methodologies. Second, the degree of crystallinity in all experiments was <25% so that enrichment in incompatible elements in the melt to progressive exclusion from the crystals would have been small. Finally, the very low values for the partition coefficients of the most incompatible elements, the HFSE, indicate that a boundary layer did not develop at the crystal–melt interface meaning that crystal growth was slow enough to maintain equilibrium partitioning at all times. As errors due to both analytical (e.g., analyzing melt inclusions in the crystal) and experimental (e.g., boundary layer development) problems should lead to partition coefficients that are biased to values closer to 1, the observation of several elements having partition coefficients in the 10^{-4} range argues strongly that neither of these aspects strongly influenced these partition coefficients.

4.2. Significance of high-T, high-An content mineral-melt D_i

Plagioclase-melt partition coefficients are particularly abundant for a significant portion of the compositional range of plagioclase (e.g., Bédard, 2006 and references therein), however high-quality plagioclase-melt partition coefficients are lacking in the high-An content range (>An_{75}). Until presently, modeling crystal fractionation or partial melting processes in which high-An plagioclase was involved required calculation of the relevant partition coefficients from regression lines projected forward formulated from and heavily weighted by abundant and scattered experimental and natural data. For example, high-An plagioclase is abundant in oceanic and continental rocks (e.g., Kimata et al., 1995; Hansen and Gronvold, 2000; Lundstrom and Tepley, 2006; Hellevang and Pedersen, 2008), and modeling either the fractionation of these crystals or the partial melting of rocks that contain these crystals require accurate and representative partition coefficients. However, as is shown by the data from this study, partition coefficients for many important trace elements between glass and high-An plagioclase generally plot lower than those projected from existing formulated regression lines. Therefore, the significance of the data and regression lines determined in this study helps users calculate more accurate partition coefficients for high-An plagioclase for use in modeling petrogenetic processes than previous studies.

4.3. Melt compositional controls on partitioning

The partitioning of trace elements between minerals and melts is known to reflect both crystal and melt composition controls (Blundy and Wood, 2003; Mysen, 2004; Huang et al., 2006). Early work on mineral-melt partitioning by Ryerson and Hess (1978) and Mysen and Virgo (1980) showed that trace elements partitioning can strongly depend on melt composition and polymerization. More recent work has stressed the importance of crystal chemical controls rather than melt structural control on trace element partitioning. Blundy and Wood (1994) and Wood and Blundy (2001) developed predictive models of trace element partitioning based on crystal-lattice strain energy, cation charge and trace element radii suggesting that plagioclase crystal chemistry strongly controls trace element partitioning in plagioclase. However, a recent study by Miller et al. (2006) specifically evaluates the role of melt composition on trace element partitioning variations in plagioclase and found that melt chemistry must be taken into consideration when evaluating partitioning behavior.

We might expect that melt compositions have some effect on the partition coefficients determined in this study. For example, the starting materials for our DAD and SDD experiments are synthetic, whereas those of the NP, SDP and AR99-2 experiments use natural rock powders. Melts from DAD and SDD have elevated CaO at ~18.5 wt.% whereas those of NP, SDP and AR99-2 are ~12–12.5 wt.% CaO. The DAD and SDD experiments produce An_{87} plagioclase, whereas the natural starting material experiments produce An_{76}, An_{74} and An_{69} plagioclase, respectively. Thus, the An_{87} plagioclase partitioning occurs between synthetic melts that differ significantly

from natural melts. Additionally, lower temperatures and lower An contents, such as those in our experiments, also typically involve melts with significantly higher degrees of polymerization. Therefore, we apply the two-lattice melt model of Nielsen and Drake (1979) and Nielsen and Dungan (1983) to our data to test whether melt has some bearing on the partitioning of trace elements into plagioclase with these experiments.

The two-lattice model of Nielsen and Drake (1979) and Nielsen and Dungan (1983) was originally constructed to reduce the dependence of trace element partition coefficients on temperature, pressure and melt composition to more accurately model igneous processes. An assumption of two-lattice models is that melt consists of two independent quasi-lattices, network formers (NF) consisting of Si, NaAl, and KAl, and network modifiers (NM) consisting of Ca, Mg, Fe, excess Al, Cr and Ti (Nielsen, 1988). The goal of this model is to create a simple melt activity model that eliminates the compositional dependence of mineral-melt partition coefficients at a constant temperature (Nielsen and Dungan, 1983).

Following the procedure of Nielsen and Dungan (1983), we converted the melt and plagioclase compositional weight data into mole fractions, and calculated a compositionally modified partition coefficient d^* which is defined as

$$d^* = X_i^{xl} / X_i^{melt} * \sum NM_{melt} \quad (12)$$

where X_i^{xl} is the mole fraction of trace element i in the crystal, X_i^{melt} is the mole fraction of trace element i in the melt, and $\sum NM_{melt}$ is the sum of the network modifiers ($AlO_{1.5}$, CaO, MgO, FeO, TiO_2) minus a portion of the network formers ($NaO_{0.5}$, $KO_{0.5}$) (Nielsen, 1985). Temperature dependence is addressed by regressing the compositionally modified partition coefficient in the form

$$\ln d^*_{obs} = a / T + b \quad (13)$$

where d^*_{obs} is the observed modified mineral-melt distribution coefficient, T is the temperature in K, a is the slope and b is the intercept of a line through the experimental data set (Nielsen, 1988). To evaluate how the two-lattice model applies to our partition coefficients and to check for internal consistency of the regression, we calculated a modified mineral-melt partition coefficient (d^*_{calc}) based on derived correlation coefficients from which expected mole fractions of trace elements in crystals were calculated using mole fractions of the melts from our experiments as unknowns. Differences between observed trace element concentrations versus calculated trace element concentrations in our plagioclase experiments reproduced in some cases to within ± 10–15%, and Fig. 5 shows an example of this case. In other cases, reproducibility was very poor, and this can be primarily attributed to analytical error associated with measuring low-concentration experiments, too few data, or errors in the two-lattice model.

Although these internal tests for consistency are variable, we provide tests of external consistency that help give validity to the evaluations. We compare the regression parameters for elements produced using the two-lattice model in this study with those derived in other studies utilizing the two-lattice model (Table 1 of Nielsen, 1990). The comparison utilizes data from this study inserted into the regression parameters and plotted as observed mole fraction of an element versus calculated mole fraction of an element (Fig. 6). The results of this comparison show that the two-lattice model regressions are quite similar even though the starting materials for each study were completely different. The conclusion is that melt compositions must be taken into consideration when using plagioclase-melt partition coefficients when modeling igneous processes, with the implication that the two-lattice model itself seems to work for a broad range of melt compositions including our experiments with synthetic starting materials.

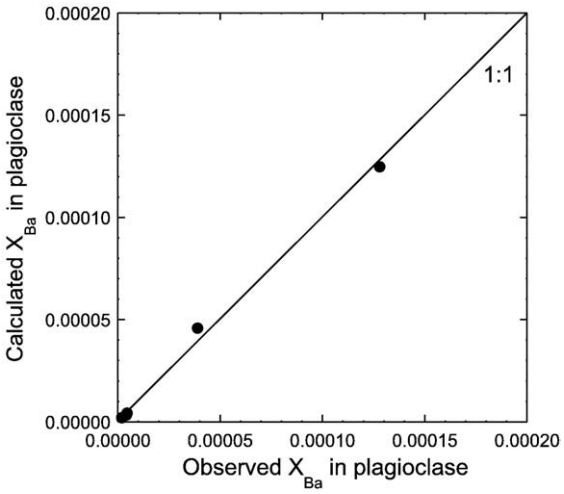

Fig. 5. Comparison of Ba concentration in plagioclase calculated from d^*_{calc} determined by linear regression model versus observed Ba concentration in the plagioclase as measured by LA-ICP-MS. Calculated values used experimental liquids as unknowns and the expressions derived from the experimental results. Solid line is the 1:1 ratio of calculated and observed, and axes are mole fractions.

From this evaluation, we have shown that melt compositional aspects must be taken into consideration when using the partition coefficients determined in this study. We have also shown that application of the two-lattice melt model to our experimentally determined partition coefficients reproduces expected trace element concentrations in plagioclase (Fig. 5). The question still remains, however, whether our high-An plagioclase partition coefficients are unusually low, in comparison to projected regressions, owing to synthetic starting materials. It is noted that the abnormally elevated CaO wt.% in the synthetic mixture experiments may have some bearing on melt chemistry affecting partition coefficients. In this regard, recent unpublished trace element partitioning data produced from natural starting materials and crystallizing An_{89} plagioclase are located in similar $RT\ln D_i$ space as this study's partitioning data (Weinsteiger et al., submitted for publication). The average CaO wt.% of melt in these experiments (12–13 wt.% CaO) is not as elevated as our synthetic experimental melts, but is similar to melt compositions in our natural powder experiments (NP, SDP; 11.8–12.5 wt.% CaO). Combined, these observations suggest that the anomalously low

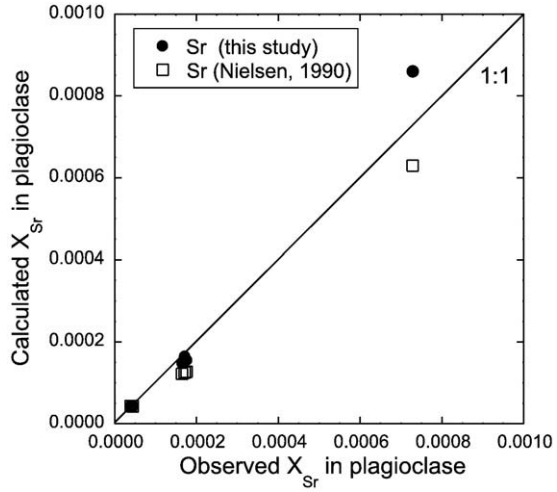

Fig. 6. Comparison of Sr concentration in plagioclase calculated from d^*_{calc} determined by linear regression model from this study and by regression in Nielsen (1990) versus observed Sr concentration in the plagioclase as measured by LA-ICP-MS. Solid line is the 1:1 ratio of calculated and observed, and axes are mole fractions.

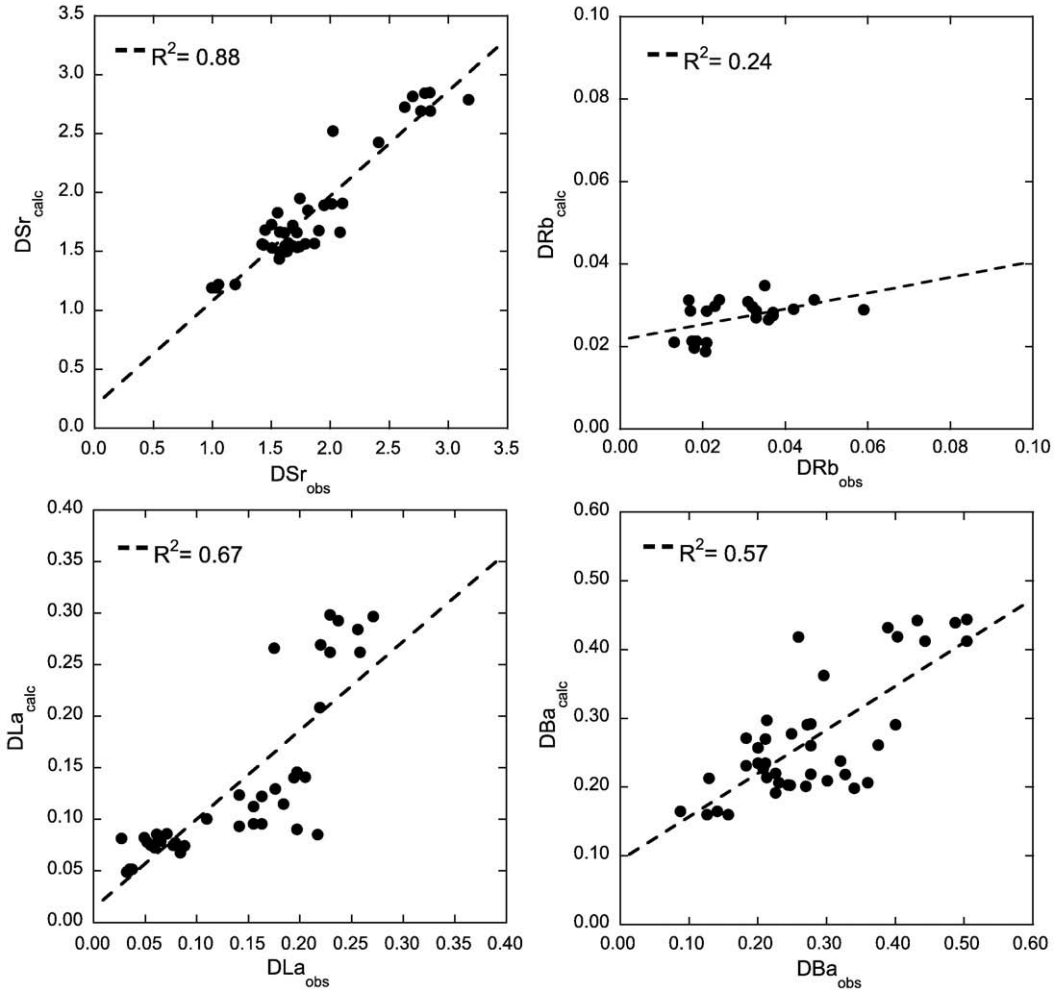

Fig. 7. Correlation between $D_{calculated}$ and $D_{observed}$ for Sr, Rb, La and Pb based on "all data" regression formulations. The use of combined data sets of plagioclase-melt partition coefficients for plagioclase composition An_{50-87} in most cases produce poorer correlations than using two separate regression formulations for plagioclase compositions An_{50-75} and An_{75-87}.

partition coefficients in the An_{87} range may be the rule rather than the exception.

4.4. New regression parameters for An_{75-87} plagioclase

Because most of our partition coefficients for high-An content plagioclase plot below multiple regression lines based on other studies, addition of our partition coefficients into the "all data" database may add considerable error to the published regressions. We determined regression parameters based on "all data", and, in most cases, the correlations are worse than if data from this study were evaluated alone (Fig. 4A–J). To quantify the error associated with these "all data" regressions, we plotted observed partition coefficients versus calculated partition coefficients where the calculated partition coefficient data were determined using the regression equations for the known An contents and the combined database "all data." Fig. 7 shows a few representative regression formulations. The correlation for D_{Sr} is very good, as would be expected given the fairly good correlation in the "all data" regression. The correlation for D_{Rb}, D_{Ba} and D_{La} are average to poor, which again follow the "all data" regressions. These observations suggest that calculating multiple linear regressions for data over a designated range in An content are necessary for determining accurate partition coefficients. In this regard, we recommend using the regressions from Bindeman et al. (1998) and Bédard (2006) for plagioclase between An_{50} to An_{75}. For plagioclase between An_{75} and An_{87}, we recommend using the regression equations from this study (Table 6). Regressions for plagioclase $>An_{87}$ will depend on future experimental work.

5. Conclusions

We determined plagioclase-melt partition coefficients for a range of trace element including light elements, LILE, REE, and HFSE by performing controlled cooling rate, 1-atmosphere experiments using both natural and synthetic basaltic (51 wt.% SiO_2) and basaltic andesite (56 wt.% SiO_2) powders doped at two different levels. The experiments were anhydrous, performed under a fO_2 approximately in the IW range and produced An_{69} to An_{87} plagioclase. Experiments produced uniform compositions in glass and crystals as determined through electron microprobe analyses. Trace elements concentrations in both glass and plagioclase were measured by SIMS and/or by LA-ICP-MS. Results for the partitioning of trace elements between plagioclase and melt at different doping levels demonstrate both adherence to Henry's Law and good agreement between the different analytical techniques.

Plagioclase-melt partition coefficients associated with plagioclase compositions An_{69}–An_{75} from this study generally show good agreement in comparison to those measured in other studies with a similar range in plagioclase composition, however partition coefficients in this study with plagioclase compositions $>An_{75}$ tend to plot lower than regressions lines projected forward from previously published regression formulations. Application of the two-lattice

model to these data and observations from ongoing partitioning studies in a similar An content range suggests that these partition coefficients are robust. Accordingly, we have formulated new regressions for the determination of plagioclase-melt partition coefficients for plagioclase compositions An_{75-87}. We suggest using the published regression formulations for plagioclase compositions An_{50-75}.

Acknowledgements

This work benefited greatly from discussions with R. Nielsen. We acknowledge I. Steele at the University of Chicago for assistance in electron microprobe analysis, and J. Baker at the Center for Microanalysis of Materials at the University of Illinois, Urbana-Champaign, for assistance in ion microprobe analysis. An informal review by R. Nielsen improved the manuscript significantly. J. Bédard and Y. Niu are thanked for providing formal reviews that also improved the manuscript significantly.

References

Aigner-Torres, M., Blundy, J., Ulmer, P., Pettke, T., 2007. Laser ablation ICPMS study of trace element partitioning between plagioclase and basaltic melts: an experimental approach. Contributions to Mineralogy and Petrology 153, 647–667.

Bartels, K.S., Kinzler, R.J., Grove, T.L., 1991. High pressure phase relations of primitive high-alumina basalts from Medicine Lake Volcano. Northern California, Contributions to Mineralogy and Petrology 108, 253–270.

Barth, M.G., Foley, S.F., Horn, I., 2002. Partial melting in Archean subduction zones: constraints from experimentally determined trace element partition coefficients between eclogitic mineral and tonalitic melts under upper mantle conditions. Precambrian Research 113, 323–340.

Beattie, P., 1994. Systematics and energetics of trace-element partitioning between olivine and silicate melts; implications for the nature of mineral/melt partitioning. Chemical Geology 117, 57–71.

Bédard, J.H., 2006. Trace element partitioning in plagioclase feldspar. Geochimica et Cosmochimica Acta 70, 3717–3742.

Bindeman, I., 2007. Erratum to I.N. Bindeman, A.M. Davis, and M.J. Drake (1998), "Ion microprobe study of plagioclase-basalt partition experiments at natural concentration levels of trace elements. Geochimica et Cosmochimica Acta 62, 1174–1193 Geochimica et Cosmochimica Acta 71, 2414.

Bindeman, I., Davis, A., 2000. Trace element partitioning between plagioclase and melt: investigation of dopant influence on partition behavior. Geochimica et Cosmochimica Acta 64, 2863–2878.

Bindeman, I., Davis, A., Drake, M., 1998. Ion microprobe study of plagioclase-basalt partition experiments at natural concentration levels of trace elements. Geochimica et Cosmochimica Acta 62, 1175–1193.

Blundy, J., Wood, B., 1991. Crystal-chemical controls on the partitioning of Sr and Ba between plagioclase feldspar, silicate melts, and hydrothermal solutions. Geochimica et Cosmochimica Acta 55, 193–209.

Blundy, J., Wood, B., 1994. Prediction of crystal-melt partition coefficients from elastic moduli. Nature 372, 452–454.

Blundy, J., Wood, B., 2003. Partitioning of trace elements between crystals and melts. Earth and Planet Science Letters 210, 383–397.

Cooper, K.M., Goldstein, S.J., Sims, K.W.W., Murrell, M.T., 2003. Uranium-series chronology of Gorda Ridge volcanism: new evidence from the 1996 eruption. Earth and Planetary Science Letters 206, 459–475.

Goldstein, S.J., Sims, K.W.W., Cooper, K.M., Murrell, M.T., Nunn, A.J., 1999. Evidence for radium–barium fractionation in mid-ocean ridge basalt plagioclase; implications for geochronology and mantle melting, LPI Contributions. Ninth Annual V.M, Goldschmidt Conference. 101.

Grove, T., Baker, M., Kinzler, R., 1984. Coupled CaAl–NaSi diffusion in plagioclase feldspar: experiments and application to cooling rate speedometry. Geochimica et Cosmochimica Acta 48, 2113–2121.

Hansen, H., Gronvold, K., 2000. Plagioclase ultraphyric basalts in Iceland: the mush of the rift. Journal of Volcanology and Geothermal Research 98, 1–32.

Hellevang, B., Pedersen, R.B., 2008. Magma ascent and crustal accretion at ultraslow-spreading ridges: constraints from plagioclase ultraphyric basalts from the Arctic Mid-Ocean Ridge. Journal of Petrology 49, 267–294.

Huang, F., Lundstrom, C.C., McDonough, W.F., 2006. Effect of melt structure on trace-element partitioning between clinopyroxene and silicic, alkaline, aluminous melts. American Mineralogist 91, 1385–1400.

Kimata, M., Nishida, N., Shimizu, M., Saito, S., Matsui, T., Arakawa, Y., 1995. Anorthite megacrysts from island arc basalt. Mineralogical Magazine 59, 1–14.

Lundstrom, C.C., Tepley III, F.J., 2006. Investigating the origin of anorthitic plagioclase through a combination of experiments and natural observations. Journal of Volcanology and Geothermal Research 157, 202–221.

Lundstrom, C.C., Shaw, H.F., Ryerson, F.J., Phinney, D.L., Gill, J.B., Williams, Q., 1994. Compositional controls on the partitioning of U, Th, Ba, Pb, Sr and Zr between clinopyroxene and haplobasaltic melts: implications for uranium series disequilibria in basalts. Earth and Planetary Science Letters 128, 407–423.

McKay, G.A., 1986. Crystal/liquid partitioning of REE in basaltic systems: extreme fractionation of REE in olivine. Geochimica et Cosmochimica Acta 50, 69–79.

McKay, G.A., Weill, D.F., 1977. KREEP petrogenesis revisited. Proceedings of the 8th lunar science conference, 2. Pergamon Press, New York, pp. 2,339–2,355.

Miller, S.A., Asimow, P.D., Burnett, D.S., 2006. Determination of melt influence on divalent element partitioning between anorthite and CMAS melts. Geochimica et Cosmochimica Acta 70, 4258–4274.

Mysen, B.O., 2004. Element partitioning between minerals and melt, melt composition, and melt structure. Chemical Geology 213, 1–16.

Mysen, B.O., Virgo, D., 1980. Trace element partitioning and melt structure: an experimental study at 1 atm pressure. Geochimica et Cosmochimica Acta 44, 1917–1930.

Nielsen, R.L., 1985. A method for the elimination of the compositional dependence of trace element distribution coefficients. Geochimica et Cosmochimica Acta 49, 1775–1779.

Nielsen, R.L., 1988. Simulation of igneous differentiation processes. In: Nicholls, J., Russell, J.K. (Eds.), Modern Methods of Igneous Petrology: Understanding Magmatic Processes, Reviews in Mineralogy, 24, pp. 65–105.

Nielsen, R.L., 1990. The use of simulated data sets for the evaluation of the sensitivity of Pearce element ratio analysis. In: Russell, J.K., Stanley, C.R. (Eds.), Theory and Application of Pearce Element Ratios to Geochemical Data Analysis, 8. Geological Association of Canada, pp. 157–178. Short Course Volume.

Nielsen, R.L., Drake, M.J., 1979. Pyroxene-melt equilibria. Geochimica et Cosmochimica Acta 43, 1259–1273.

Nielsen, R.L., Dungan, M.A., 1983. Low pressure mineral-melt equilibria in natural anhydrous mafic systems. Contributions to Mineralogy and Petrology 84, 310–326.

Ringwood, A.E., 1970. Petrogenesis of Apollo 11 basalts and implications for lunar origin. Journal of Geophysical Research 75, 6,453–6,479.

Ryder, C.H., Gill, J.B., Tepley III, F.J., Ramos, F., Reagan, M., 2006. Closed- to open-system differentiation at Arenal volcano (1967–2003). Journal of Volcanology and Geothermal Research 157, 75–93.

Ryerson, F.J., Hess, P.C., 1978. Implications of liquid–liquid distribution coefficients to mineral–liquid partitioning. Geochimica et Cosmochimica Acta 42, 921–932.

Shimizu, N., Semet, M.P., Allegre, C.J., 1978. Geochemical applications of quantitative ion-microprobe analysis. Geochimica et Cosmochimica Acta 42, 1321–1334.

Steele, I.M., Peters, M.T., Shaffer, E.E., Burnett, D., 1997. Minor element partitioning and sector zoning in synthetic and meteoritic anorthite. Geochimica et Cosmochimica Acta 61, 415–423.

Tormey, D.R., Grove, T.L., Bryan, W.B., 1987. Experimental petrology of normal MORB near the Kane Fracture Zone: 22°–25° N, mid-Atlantic ridge. Contributions to Mineralogy and Petrology 96, 121–139.

van Westrenen, W., Draper, D.S., 2007. Quantifying garnet-melt trace element partitioning using lattice strain theory: new crystal-chemical and thermodynamic constraints. Contributions to Mineralogy and Petrology 154, 717–730.

Watson, E.B., 1985. Henry's Law behavior in simple systems and in magmas: criteria for discerning concentration-dependent partition coefficients in nature. Geochimica et Cosmochimica Acta 49, 917–923.

Weill, D.F., McKay, G.A., 1975. The partitioning of Mg, Fe, Sr, Ce, Sm, Eu, and Yb in lunar igneous systems and a possible origin of KREEP by equilibrium partial melts. In: Merrill, R.B., Hubbard, N.J., Mendell, W.W., Williams, R.J. (Eds.), Proceedings of the 6th Lunar Science Conference, 1. Pergamon Press, New York, pp. 1,143–1,158.

Weinsteiger, A., Neilsen, R., Kent, A., Tepley, F.J., III, (submitted for publication) The trace element diversity of anorthitic MORB plagioclase and their associated melt inclusions.

Wood, B.J., Blundy, J.D., 2001. The effect of cation charge on crystal-melt partitioning of trace elements. Earth and Planetary science Letters 188, 59–71.

Zinner, E., Crozaz, G., 1986. A method for the quantitative measurement of rare earth elements in the ion microprobe. International Journal of Mass Spectrometry Ion Processes 69, 17–38.